Automated multifilter rotating shadow-band radiometer: an instrument for optical depth and radiation measurements

Lee Harrison, Joseph Michalsky, and Jerry Berndt

The multifilter rotating shadow-band radiometer is a ground-based instrument that uses independent interference-filter–photodiode detectors and the automated rotating shadow-band technique to make spectrally resolved measurements at seven wavelength passbands (chosen at the time of manufacture between 350 nm and 1.7 μm) of direct-normal, total-horizontal, and diffuse-horizontal irradiances. This instrument achieves an accuracy in direct-normal spectral irradiance comparable with that of tracking radiometers, and it is more accurate than conventional instruments for the determination of the diffuse and total-horizontal spectral irradiances because the angular acceptance function of the instrument closely approximates the ideal cosine response, and because the measured direct-normal component can be corrected for the remaining angular acceptance error. The three irradiance components are measured with the same detector for a given wavelength. Together with the automated shadow-band technique, this guarantees that the calibration coefficients are identical for each, thus reducing errors when one compares them (as opposed to measurements made with independent instruments). One can use the direct-normal component observations for Langley analysis to obtain depths and to provide an ongoing calibration against the solar constant by extrapolation to zero air mass. Thus the long-term stability of all three measured components can be tied to the solar constant by an analysis of the routinely collected data.

Key words: Atmospheric radiometry, turbidity, optical depth, Langley regression.

Automated Rotating Shadow-Band Radiometry

The basic geometry of a computer-controlled rotating shadow-band radiometer can be seen in Fig. 1. The shadowing band is a strip of metal formed into a circular arc that lies along a celestial meridian (the face of the Lambertian detector is the center for this arc). It can be accurately rotated in 0.4° steps around the polar axis by a direct-coupled stepping motor that is in turn controlled by a microprocessor. This band blocks a strip of sky with an umbral angle (Zp)[1] of 3.27°, which is more than sufficient to block the solar disk. The tracking accuracy must be substantially better than Zp because of the presence of the solar aureole within the field of view. For this instrument the limiting accuracy is ±0.3° because of stepping precision and error. (Contributions from an allowance for approximately 1° of misalignment of the polar axis and the computational accuracy of the ephemeris are negligible in comparison.) The mechanism permits a simple mechanical adjustment for the latitude. This adjustment, together with the azimuth alignment to the Earth's pole (of either the northern or southern hemisphere, depending on the site latitude), is done when the instrument is installed at a site; no further mechanical adjustment is necessary.

The operation of the instrument is controlled by its self-contained microprocessor. At each measurement interval it computes the solar position by using an approximation for the solar ephemeris. The measurement sequence starts with a measurement made while the band is at nadir; this is the total-horizontal irradiance. The band is then rotated so that three measurements are made in sequence; the middle one blocks the Sun and the other two block strips of sky 9° to either side. These side measurements permit a first-order correction for the excess sky blocked by the band when the Sun-blocking measurement is made. One subtracts the average of these two side measure-

J. Berndt is with the Pacific Northwest Laboratory, P.O. Box 999, Richland, Washington 99352; the other authors are with the Atmospheric Sciences Research Center, State University of New York at Albany, 100 Fuller Road, Albany, New York 12205.

Received 25 January 1993; revised manuscript received 4 February 1994.

0003-6935/94/225118-08$06.00/0.

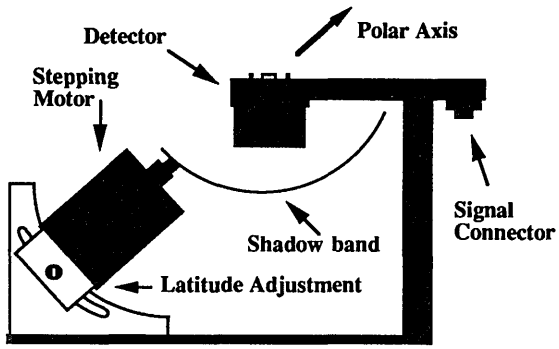

Fig. 1. Basic geometry of an automated rotating shadow band (shown in the position where the measurement of the total-horizontal irradiance is made).

ments from the total-horizontal measurement and then adds this correction to the Sun-blocked measurement to determine the diffuse-horizontal irradiance. The 9° offset must be larger than one half of angle $Z1$ (see Table 1) plus one half of the solar disk, or $\approx 6.75°$. (Modeling demonstrated that 9° yields a better first-order correction for sky radiances expected with typical optical depths and scattering phase functions, given the Zp angle of 3.27°.) Finally, one can subtract the diffuse component of the irradiance from the total-horizontal component to produce the direct-horizontal component. Division by cosine of the solar position angle from the zenith (available from the ephemeris calculation) then produces the direct-beam flux on a normal surface. The entire measurement sequence is completed in less than 10 s and is normally programmed to occur four times per minute.

The microprocessor also acts as a data logger, accumulating the data from the shadow-band measurements as well as from ancillary measurements from other instruments if desired. All analog signals have conditioning amplifiers as needed, and they are multiplexed to an analog-to-digital converter with 12-bit-plus sign resolution (1 part in 8192) and 1-bit reproducibility over the range from −4.096 to 4.095 V. The instrument can average over selected intervals; note that in this case the summation of the direct-normal component is done subsequent to the division by the cosine of the solar zenith angle (which is done individually for each measurement). This is necessary to produce correct results at high solar zenith angles in which the cosine varies rapidly. The instrument stores and telemeters data and has a battery backup so that operation continues through power outages.

The basic rotating blocking-band method was developed by Wesely.[2] Instruments have since been developed[3,4] to automate the Wesely method. The multifilter rotating shadow-band radiometer (MFRSR) differs from these in that it uses a computed ephemeris to position the band for the blocking measurements and does not depend on the detection of a minimum irradiance. This method permits much longer integration times for each measurement because it requires measurements at only four positions rather than a continuous scan across the sky. This substantially improves measurement precision and permits what would otherwise be impossible wavelengths or passbands. The excess sky blockage correction also significantly improves the measurement accuracy, particularly under skies with fractional cloud coverage. A disadvantage is that the instrument must be properly aligned. (The instrument developed by Guzzi *et al.*[3] was intended for shipborne application, where no such alignment was possible.)

Blocking-band techniques have several advantages over the traditional alternative of using two detectors, one fixed to measure the total-horizontal irradiance, and one mounted on a tracking mechanism to measure the direct-normal component (thus requiring a narrow field of view). They are simpler, less expensive, and more robust. Further, the three irradiance components are derived from a single optical detector, greatly reducing our intercalibration worries over both absolute sensitivity and spectral passband and guaranteeing that the measurements are synchronous. These features improve the utility of calibration by means of Langley extrapolation (discussed below), because the measurements of the diffuse- and total-horizontal irradiances are calibrated as well.

Table 1. Field-of-View Full Angles[a]

Instrument	Zp (deg)	$Z0$ (deg)	$Z1$ (deg)
MFRSR	3.274	8.172	13.04
Tracking radiometer	3.53	5.73	7.92

[a]Angles Zp, $Z0$, and $Z1$ are defined in Ref. 1.

Seven-Passband Lambertian Detector

Radiometers intended to measure the flux incident on a surface must measure the input from a 2π sr field of view, weighted by the cosine of the incidence angle from the surface norm. This ideal response is described as Lambertian. The empirical development of Lambertian diffusers optimized for various wavelengths is not new; by the time of the early research of Kerr *et al.*,[5] it was recognized that simple glass domes covering flat-plate detectors did not perform well (particularly at solar zenith angles greater than 70°), and that flat diffusing receivers with carefully shaped sidewall and blocking-ring geometries were superior.

The performance of the inlet optic with respect to the correct integration over the sky radiance distribution is critical for many uses of the data and has been a continuing problem in radiometry. Many commonly used radiometers have angular response functions that deviate from the ideal by more than 20% at some angles, and often these angular response functions do not reproduce well from unit to unit of a single design. In addition to the need for good optical performance, however, there are practical constraints stemming from the requirement that the inlet optic be suitable for field use. The optic must have a sealed entrance and must be designed both to

be readily cleaned and to minimize the optical consequences of small (but inevitable) soiling. It also must be designed to avoid aging degradation.

Figure 2 shows the design of our multifilter detector assembly. The exterior, except for the optical inlet, is black-anodized aluminum. The optical inlet is a protruding diffuser surrounded by a raised blocking ring. (Not shown is a drain hole that prevents rainfall or melted ice from filling the annular well between the optical inlet and the blocking ring.) The diffuser is made of Spectralon, a proprietary optical plastic manufactured by Labsphere. The thin-walled external button acts as a transmission diffuser, and the thick internal sidewalls form a partial integrating cavity. Two diaphragms of Schott Glaswerke frosted WG-280 glass act as transmission diffusers so that the randomization of the photon trajectories is increased. We arrived at the geometry of the protruding diffuser, the sidewall blocking rings, and the integrating cavity by extensive empirical optimization (cut and try), using the automated test facility described below.

Spectralon is a halocarbon with excellent resistance to chemical and ultraviolet degradation. (The material must be baked *in vacuo* at 90° C for several hours to drive off residual oils from manufacture. After this the material shows excellent resistance to weathering and irradiation.[6]) Consequently, we believe that these detectors will have stable long-term performance in the field environment. In addition, diffusers are inherently less sensitive to surface soiling by typical atmospheric aerosols than are transmission windows (e.g., instruments with domes such as thermopile pyranometers). The reason is that the deposition of a small increment in scattering on the surface of the diffuser makes a negligible change in its throughput because the optical depth is already large. In contrast, transmission of a window is affected linearly. The single-scattering albedo of most natural aerosols is in excess of 0.9 (except soot); their deposition does not substantially affect an optically thick diffuser coupled to an integrating cavity.

The entire detector consists of the diffuser–integrator described above that illuminates an internal hexagonal close-packed array of seven photodiodes with interference filters. These diodes are mounted to the interior of a five-sided cubic printed circuit board that provides a separate transimpedance amplifier (zero-bias current-to-voltage amplifier) for each of the photodiodes. We use an alignment tool to position them during soldering so that the face of each is normal to, and centered on, a line from the center of the exit aperture of the diffuser. No ray entering the filter is more than 7.5° from normal. The circuit-board assembly mounts to an internal aluminum shroud that has a grooved and anodized surface that reduces stray trajectories to the detectors, which also serves as the support for the heating strip (not shown).

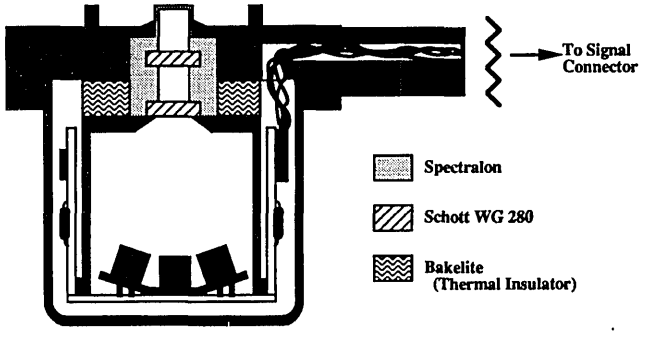

Fig. 2. Multifilter detector cross section (not to scale).

We operate the photodiodes in the photovoltaic (rather than photoconductive) mode to reduce noise and increase sensitivity and stability. We implement transimpedance amplifiers by using individual Linear Technologies LTC1050 commutating-autozero (i.e., chopper-stabilized) devices to reduce variations in input offset and bias current. The amplifier for each channel has a first-order feedback time constant that is set from 0.02 to 0.06 s. The motion algorithm guarantees that the band has been stationary for 1 s before any of the channels are sampled; this ensures that the signal has settled well beyond the accuracy of the digitization.

The interior of the detector assembly is thermally insulated with a phenolic spacer around the diffuser and with a Kapton film with glass wool insulation around the electronics. It has a thermostatic electrical heater (25-W maximum) that holds the temperature of the internal detector assembly at a set point from 35 °C to 45 °C (for hot sites). Temperature stabilization is necessary to improve the accuracy in several ways. Both the passband and transmission of interference filters are sensitive to temperature, although these effects are most pronounced with passbands that are significantly narrower than those we employ. More importantly, the photodiodes exhibit changes in sensitivity with temperature, and the bias currents of the amplifiers are temperature sensitive as well. Finally, the elevated and stable temperature improves the long-term stability of the interference filters by eliminating temperature-cycle-induced mechanical fatigue of the dielectric lamina (that have differing expansion coefficients) and by guaranteeing a low internal humidity. (Provision is made for an additional desiccator for environments that are warm and humid.) An important operational side benefit of this temperature control is that the heat loss keeps the detector ice free in all but the worst icing conditions.

Silicon photodiodes are optimum over the wavelength range 350–1000 nm. We currently use DF Series integrated photodiode–interference-filter assemblies manufactured by EG&G Optoelectronics. The typical detector photocurrent is wavelength dependent, but it nears 1 nA for a 10-nm passband at wavelengths below 380 nm. We require at least 1 part in 10^3 sensitivity and precision, which in turn requires picoampere current stability. Beyond 1050 nm either germanium or indium gallium arsenide photodiodes are required. As a result of a decreasing

irradiance at longer wavelengths and poorer shunt resistance of the detectors, passbands greater than 20 nm are needed at wavelengths beyond 1.3 μm.

The MFRSR instruments built for the Atmospheric Radiation Measurement and Quantitative Links experiments have six filtered detectors with a nominal 10-nm FWHM bandwidth at wavelengths of 415, 500, 610, 665, 862, and 940 nm and an unfiltered silicon photodiode. The filtered passband curves are shown in Fig. 3. We measure these simultaneously, testing the complete detector assembly as a unit, and they demonstrate the expected small shift and broadening of the passbands compared with those of the same filters tested at uniform normal incidence. We choose all the filtered passbands except 940 nm (a water-vapor band) to permit a Langley analysis for the direct determination of optical depth. We choose the wavelengths to span a useful range for flux calculations and to permit the maximum amount of information about the aerosol extinction to be retrieved through inversions.[7–9] An additional goal (that we have yet to demonstrate) is the estimation of column ozone from Chappuis band absorption.

Lambertian Performance

We constructed an automated test facility to measure the angular response functions of detectors.[10] The light source is a 300-W, 1-in.- (2.54-cm-) aperture axial xenon arc with an encapsulated parabolic rear reflector and a plane exit window (by ILC Corporation). This produces an output beam with residual polarization less than 1%. We project this through a 5.08-m-long, black-walled tube with internal baffles to eliminate off-axis light, to an enclosed black-walled working cavity with a 70-cm working swing radius around the central beam point. The working optical aperture is slightly greater than 5 cm in diameter, with a measured intensity uniformity of better than 1%. The maximum beam divergence is 0.5°, with 84% of the radiance having a beam divergence of less than 0.25°. The calibration process is automated by a computer that controls the angular rotation of the apparatus under test and that also samples and stores the detector output. Such automation is critical to the development of good Lambertian detectors (particularly if they must operate over a range of wavelengths), because repeated measurements (and some cut-and-try iteration) are required for us to arrive at an acceptable design. We need repeated back-and-forth scans to average the inevitable lamp fluctuations of the xenon arc.

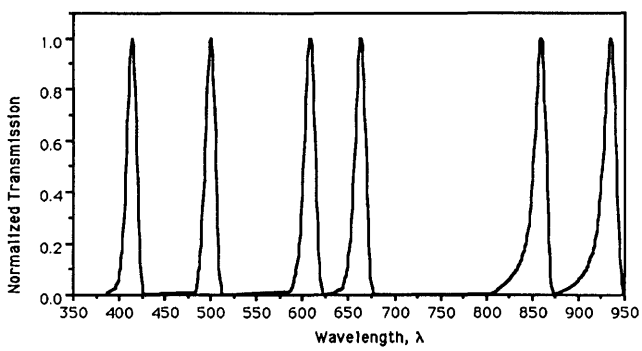

Fig. 3. Filtered passbands of the MFRSR.

Measurements are made from −90° to 90° (with respect to the normal axis of the detector) along two orthogonal planes corresponding to the east–west and north–south azimuth orientation in the field. The measurement at two independent azimuth orientations make any azimuthal dependence of the detector apparent, and it permits an accurate correction of the direct-beam component for the remaining deviations in the angular response function. This is of particular importance for the correct determination of optical depths.

A major part of our development effort for the multifilter instrument was the development of the diffuser geometry. We need adequate light throughput, good approximation to an ideal cosine response at all wavelengths, and low azimuthal variation. In addition, a practical requirement is reproducible cosine behavior within the limits of achievable manufacturing tolerances. We found these goals to be much more difficult for a design that must illuminate multiple-interference filters at near-normal incidence (implying a substantial standoff distance from the exit aperture to the filter) than for a simple diffuser with a large-area diode immediately behind (as is typical of single-passband designs). Initial guesses for trial geometries were based on Monte Carlo ray-tracing simulations, but the lack of accurate data concerning the scattering phase functions and absorption coefficients of our optical media prevented these from being anything more than the starting point for experimental iteration. Early designs had strong azimuthal dependence because of the diode position. (The first test of each design is done with identical unfiltered detectors in all seven positions.) Most of our effort was directed toward minimizing this effect while retaining adequate light throughput. Once results similar to those shown below were achieved in azimuthal dependence, then minor tailoring of thickness and height ratios optimized the Lambertian behavior over the wavelength range.

The performance of our diffuser geometry for all seven passbands is shown in the graphs of Figs. 4a and 4b, which show error ratios for each of the passbands for the two orthogonal scans. Figure 4(c), for comparison, shows three Eppley PSP instruments. At all wavelengths the cosine response of our diffuser is competitive with the best single-passband scientific instruments. We have the design freedom to trade off errors to some extent. Our primary criterion is to produce correct total irradiance for typical diffuse skies (as we discuss further below), because we can correct the direct-beam component. Additional considerations are maintaining smooth correction functions through the zenith angles used for Langley extrapolation to decrease the sensitivity of these calculations to the corrections, and, of course, the sensitivity to manufacturing tolerances.

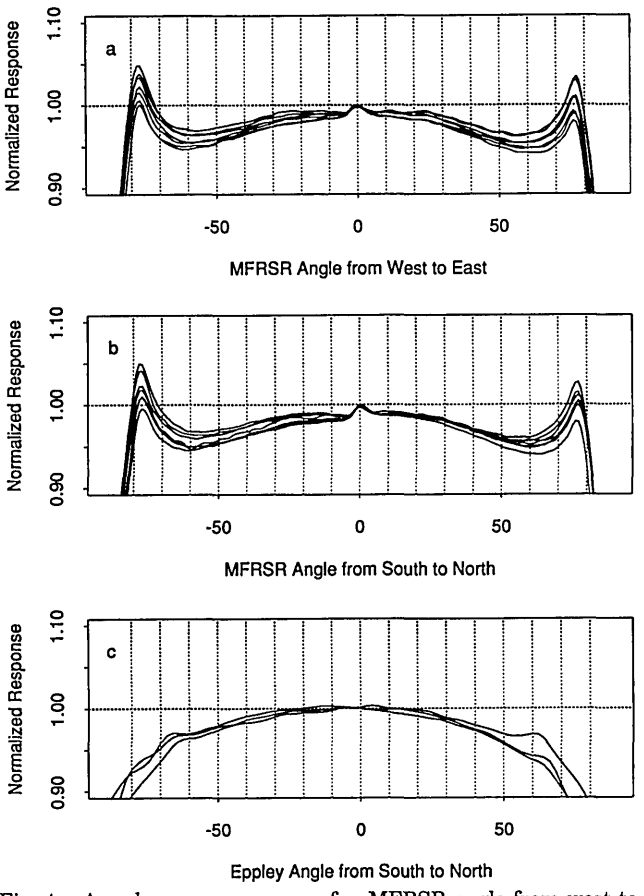

Fig. 4. Angular response error of a, MFRSR angle from west to east; b, MFRSR angle from north to south, both for seven passbands; c, Eppley PSP angle from south to north.

Laboratory radiometric calibrations are usually done at normal incidence only; this is physically the least interesting angle. When the Sun is visible the irradiance is dominated by the direct beam, and hence the instantaneous solar zenith angle is the most important one. Rarely is it at the zenith. For diffuse skies the total flux is given by the integral

$$\Phi = \int_0^{\pi/2} L(\theta)\cos(\theta)\sin(\theta)\mathrm{d}\theta,$$

where $L(\theta)$ is the almucantar-averaged radiance as a function of zenith angle θ. Function $\cos(\theta)\sin(\theta)$ peaks at 45°. Realistic diffuse skies exhibit a zenith brightness (a consequence of the ground albedo being <1), but this rarely decreases the zenith angle of the peak contribution to the flux integral to $<35°$. If the angular response cannot be ideal, then a response function that mildly overcompensates at high zenith angles (so that midrange angles near 45° are more accurate) is substantially better at producing correct flux integrals than a response such as that of the Eppley PSP that monotonically declines at increasing zenith angles.

The angular misalignment error between the actual optical axis of the instrument and the geometric axis can be estimated by the mean angle of the measured angular irradiance function.

$$\theta_{\mathrm{error}} = \frac{\int_{-\pi/2}^{\pi/2} E(\theta)\theta\mathrm{d}\theta}{\int_{-\pi/2}^{\pi/2} E(\theta)\mathrm{d}\theta}.$$

This is the maximum-likelihood estimator, if we are given uncorrelated normally distributed measurement errors. The small residual azimuthal variations among the passbands (caused by diode positions around the outer hexagon) are well modeled as an individual plane tilt relative to the normal optical axis. These angles typically range from $\approx 0.01°$ to 0.5°, and they are comparable with those of single-passband instruments.[10]

If left uncorrected, tilt errors can be important to a measurement error budget when high accuracy is required. A 0.25° error in east–west alignment (i.e., hour angle) corresponds to 1 min of time. Errors in inferred direct-beam components and the resulting computation of optical depth are sensitive to such errors.[11] In contrast, the diffuse-sky irradiances are less affected. The error is $\sin(\theta_{\mathrm{error}})$ for the artificial case of a uniform sky irradiance and a zero surface albedo: in this case an error of 0.25° in the zenith axis causes an error of 0.5%. [This error is not negligible when judged against the admittedly difficult goal of the Atmospheric Radiation Measurement (ARM) program for measurement accuracies better than 1%.] The sensitivity of the measurements to small tilts demonstrates the need for accurate characterization of the detector response, careful alignment of the instrument in the field, and concern about its long-term stability. Correction of the data (as described below) based on the measured angular responses as well as a leveling accuracy of 0.1° is required for reduction of these errors so that they make a small contribution to a 1% budget. (The detector head is designed for the provision of a large flat fiducial leveling surface, and all measurements, both in the laboratory and the field, are referenced to it. This also illustrates the great difficulty of making accurate observations from ships, or even meteorological towers. Many buildings sway more than 0.1°, either from wind loads or from the diurnal thermal cycle.)

Example Data

Figure 5a shows the time series of direct-beam irradiances measured by a MFRSR at the Rattlesnake Mountain Observatory (RMO, 46.40° N, 119.60° W, elevation 1088 m) on 6 October 1992. The direct-beam irradiance is derived by difference; thus it is the most sensitive to experimental error. We chose this day for presentation because it had a clear interval in the morning for Langley regression and scattered cloud passages in the afternoon. Figure 5b shows the morning Langley plots for all the filtered pass-

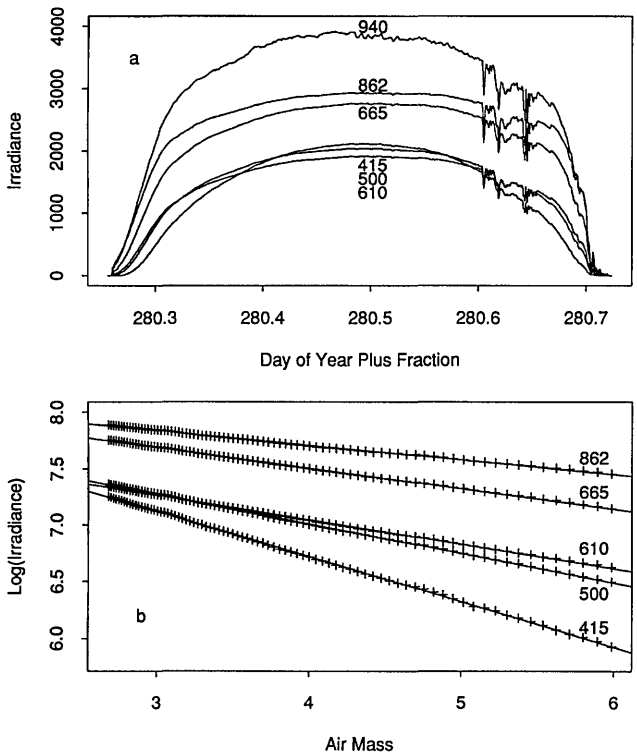

Fig. 5. a, Time series of MFRSR data for one day; b, associated Langley regressions.

bands except 940 nm, for which this method of optical depth analysis is inappropriate. The direct-beam component has been corrected for the remaining angular error of the detector as described below, and we performed Langley analyses by using algorithms described by Harrison and Michalsky.[12] The linearity of the regressions demonstrates the accuracy to which this can be done. The total optical depths retrieved for these cases are shown in Table 2.

Correction of the Direct-Normal Irradiance for Lambertian Receiver Error

The direct-normal irradiance can be corrected for the residual errors of the Lambertian receiver, provided that adequate calibrations such as those shown above are available. There are two reasons for us to make these corrections: the direct-normal irradiance must be corrected for us to obtain accurate optical depth retrievals, and the accuracy of the estimation of the total-horizontal measurement can be improved when a direct beam is present.

Table 2. Total Optical Depths (τ) at the RMO

Wavelength (10-nm FWHM)	Optical Depth (τ)	
	MFRSR	Tracking Radiometer
415	0.402	0.408
500	0.265	0.262
610	0.220	0.221
665	0.184	0.182
862	0.130	0.133

This is similar to the method routinely used for the improvement of pyranometer measurements of total-horizontal irradiance; data taken with a shaded pyranometer measure the diffuse component, and a second narrow-field-of-view normal-incidence pyranometer measures the direct beam. One then aggregates the results by using the known cosine of the zenith angle,

$$E_{\text{total-horiz}} = E_{\text{diffuse}} + \cos(Z)^* E_{\text{direct-normal}}.$$

With the MFRSR one needs only a single instrument, thereby avoiding the problem inherent in this method of matching the calibrations if two independent detectors are used for the separate components.

The correction of the direct-normal irradiance is done to each observation as table-directed linear interpolation from the angular calibrations shown above. The solar azimuth angle is resolved into the four quadrants, and then zenith-angle dependence is proportioned from the two orthogonal axes of measurement linearly with respect to angle (the north-to-east quadrant equation):

$$C(\phi, \theta) = \frac{90 - \phi}{90} \frac{1}{f_{\text{north}}(\theta)} + \frac{\phi}{90} \frac{1}{f_{\text{east}}(\theta)}.$$

Here C is a multiplying correction factor, θ is the solar zenith angle, ϕ is the solar azimuth angle in degrees, and f_{north} and f_{east} are the normalized angular response functions shown in Figs. 4a and 4b. We retain tables for each instrument, storing the f values along the four quadrant axes at 1° increments, and we linearly interpolate in between. This interpolation scheme is accurate for Lambertian receivers that do not show strong azimuthal variation, and in which the effective tilt of the optical axis as discussed above is sufficiently small that the approximation $\sin(x) \approx x$ is valid. If the effective tilt is larger, then two-step interpolations based on the resolved projection axes of the solar position in Cartesian coordinates followed by separate corrections for effective tilt (as estimated above) and then residual diffuser errors would be needed. Characterization of the receiver along more than two azimuthal axes would be required if the variation were larger.

Intercomparison with Sun-Tracking Radiometry

The MFRSR at RMO also acquires data from a seven-passband tracking radiometer. We constructed this instrument by placing a multifilter detector assembly (including the housing and diffuser) at the end of a tube with an entrance aperture; we selected the length and aperture size to mimic the acceptance angles of the Eppley normal incidence pyranometer. The angles for the tracking radiometer and MFRSR are shown in Table 1. This radiometer is continuously pointed at the Sun by a LiCor solar tracker. Our purpose for this detector is to demonstrate the accuracy of the optical depths retrieved from the MFRSR. Intercomparison of the data from the MFRSR with that from the tracking instrument tests

Table 3. Correlation Coefficients for Optical Depths Retrieved by Colocated MFRSR's and Tracking Radiometers

Passband Center (nm)	Correlation Coefficient
415	0.92
500	0.95
610	0.97
665	0.97
862	0.97

the entire MFRSR measurement system, including all the calibration and correction algorithms.

Close matching of passbands must be maintained for any intercomparison of optical depths. All instruments will intrinsically measure the total optical depth, although in most cases it is only the variable aerosol and trace-gas components that are of interest, for which the Rayleigh extinction is subtracted. However, mismatch in perceived optical depth is dominated by the Rayleigh contribution, both because it is the dominant extinction process at all but the longest wavelengths and because it has the strongest wavelength dependence, varying as λ^{-4} for

$$\tau = C\lambda^{-a},$$

the differential

$$\left(\frac{d\tau}{\tau}\right) = -a\left(\frac{d\lambda}{\lambda}\right).$$

Consequently, for a passband at 500 nm, a wavelength accuracy of ≈ 1 nm is required for us to obtain 1% accuracy in the determination of total optical depths.

The results of the intercomparison of optical depths retrieved by the MFRSR with those from narrow-field-of-view tracking detectors are shown in Table 3 and Fig. 6. Table 3 shows the correlation coefficients between the two instruments for inferred optical depths. Figure 6 shows the statistics of aggregated measurements for the assessment of the bias. The bias between the two instruments is smaller than

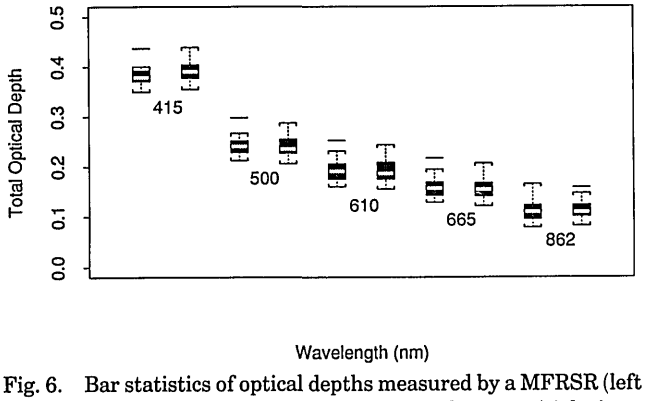

Fig. 6. Bar statistics of optical depths measured by a MFRSR (left item of each passband pair) and a tracking radiometer (right item of each passband pair). Central boxes represent the central 50% of the data; white central bars represent the median. Dashed lines and vertical brackets illustrate the extrema.

that expected because of an assumed limit of passband-matching accuracy of 1 nm for all wavelengths except 415 nm, and it is comparable with this limit for the 415-nm passband.

Worst-case estimates of the accuracy of the optical depths inferred by this shadow-band technique can be derived easily from the statistics in Table 3 and Figure 6, if we assume that all variation is to be attributed to the shadow-band measurements. In this case the standard error of the inferred optical depths is approximately 0.0125 for measurements at 500 nm and 0.0055 for those at 610 nm. (Statistics are presented for these wavelengths for the purpose of comparison against the World Meteorological Organization standard of 0.05 optical depth for photopic measurements.) More realistic estimates involve some discretion in analysis, but they plausibly regress to remove residual bias caused by wavelength mismatch and attempt to apportion the variance in retrieved optical depths between the two measurements on the basis of variance observed within the Langley regression. In this case the standard errors are reduced by slightly more than $2^{-1/2}$ and are comparable for both measurement technologies.

Optical depths become highly variable when the total extinction is dominated by large particles, e.g., thin cirrus. In this case, differing effective fields of view of the direct-beam measurements (see Table 1) change the perceived optical depth because of the large fraction of light scattered into small forward angles by particles that are large compared with the wavelength. The larger effective field of view of the MFRSR would cause it to report a smaller optical depth. However, these cases are readily identified by the noise in the Langley regression caused by the spatial and temporal variability of such clouds, and because the non-Rayleigh extinction becomes nearly independent of the wavelength. These signatures provide a ready indicator of the presence of subvisual clouds; Langley optical depths inferred from either instrument are normally discarded.

In Situ Calibrations That Use Air-Mass Extrapolation

In Figs. 5a and 5b the irradiance scale is uncalibrated (it is simply digitized millivolts). The Langley regression for the determination of optical depth is a ratiometric method that does not depend on an absolute calibration. A second major use of the Langley analysis is in the attainment of the extrapolated intercept of this regression with zero air mass, E_0. When corrected for the variation in the Earth–Sun distance ($E_0{}^*A^2$, where A is the distance from the Earth to the Sun in astronomical units), this value is the inferred solar constant at the passband. Attainment of this value requires an extrapolation of at least one air mass, so small errors in τ can cause much larger errors in E_0.

At exceptional sites (e.g., Mauna Loa) individual Langley regressions taken under favorable conditions will show variations in $E_0{}^*A^2$ of less than 1%. This is remarkable and exceeds the precision of all but the

best laboratory spectral calibrations. More typical sites show much larger variations in the extrapolated E_0. Single regressions, then, do not yield good estimates. However, these variations are not systematic, and we demonstrate[12] that it is feasible for us to obtain calibrations against the solar constant by averaging the results of a series of regressions. This was done at a site atop the National Oceanic and Atmospheric Administration complex within the Denver, Colorado, basin; this is a site known as a difficult one and that is considered unsuitable for photometer intercomparisons, both because of variable air-mass trajectories across the front range to the west and because of local flows that perturb the urban pollution. Thus if the instrument has adequate short-term stability to permit the acquisition of a sufficient number of Langley extrapolations (under all but the most unfavorable conditions in less than 3 months), then the long-term stability of calibration can be maintained by an analysis of the returned data to a precision of approximately 1%. The absolute accuracy depends on the precision to which the passband is known, and the accuracy and stability of the solar constant.

Conclusions

The MFRSR is a single instrument that can replace a suite of standard instruments. It provides spectrally resolved measurements at seven passbands of the direct-normal, diffuse-horizontal, and total-horizontal irradiance. Demonstrated accuracies are comparable with tracking instruments for the direct-normal components (and thus optical depths), and they are superior to those of existing Lambertian radiometers for the diffuse-horizontal and total-horizontal irradiances. An important advantage of the MFRSR is that the diffuse- and total-horizontal irradiance measurements are guaranteed to have the same passband and sensitivity as the direct-normal irradiances. This greatly reduces the errors in analyses that compare these components (versus traditional measurement techniques that require separate instruments), and it permits the measurements of total- and diffuse-horizontal irradiances as a way to share the utility of long-term calibration by Langley regression and zero-air-mass extrapolation. MFRSR's are currently being deployed by both the Quantitative Links measurement program and at the Clouds and Radiation Testbed sites of the ARM program. Instruments are also being used in the Tropical Oceans-Global Atmosphere, Coupled Ocean-Atmosphere Response experiment and are being deployed by individual investigators as well.

Research at the Atmospheric Sciences Research Center was supported by the U.S. Department of Energy (DOE) Quantitative Links program and through grant DE-FG02-90ER61072 (ARM program), and by the New York State Energy Research and Development Authority under grant 1725-EEED-IEA-92. At Pacific Northwest Laboratory the research was supported by the Quantitative Links program and the Office of Basic Energy Sciences within the DOE. The Pacific Northwest Laboratory is operated for the DOE by Battelle Memorial Institute under contract DE-AC06-76FLO 1830.

References and Notes

1. M. Iqbal, *An Introduction to Solar Radiation* (Academic, New York, 1983). Note that Fig. 12.5.1 of Iqbal shows definitions of the half angles, whereas his associated table, Table 12.5.1, shows full angles = 2* half angles. The *Zp*, or umbral angle, is of particular importance for a blocking method because it is the angle for which every point on the detector is blocked.
2. M. L. Wesely, "Simplified techniques to study components of solar radiation under haze and clouds," J. Appl. Meteorol **21,** 373–383 (1982).
3. R. Guzzi, G. C. Maracci, R. Rizzi, and A. Sicardi, "Spectroradiometer for ground-based measurements related to remote sensing in the visible from a satellite," Appl. Opt. **24,** 2859–2863 (1985).
4. T. Stoffel, C. Riordan, and J. Bigger, "Joint EPRI/SERI project to evaluate solar energy radiation measurement systems for electric utility solar radiation resource assessment," in *Proceedings of the IEEE Photovoltaic Specialist's Conference* (Institute of Electrical and Electronics Engineers, New York, 1991).
5. J. P. Kerr, G. W. Thurtell, and C. B. Tanner, "An integrating pyranometer for climatological observer stations and mesoscale networks," J. Appl. Meteorol. **6,** 688–694 (1967).
6. A. E. Stiegman, C. J. Bruegge, and A. W. Springsteen, "UV stability and contamination analysis of Spectralon diffuse reflectance material," Opt. Eng. **32,** 799–804 (1993).
7. M. D. King, D. M. Byrne, B. M. Herman, and J. A. Reagan, "Aerosol size distributions obtained by inversion of spectral optical depth measurements," J. Atmos. Sci. **35,** 2153–2167 (1978).
8. M. D. King and B. M. Herman, "Determination of the ground albedo and the index of absorption of atmospheric particles by remote sensing, part 1: theory," J. Atmos. Sci. **36,** 163–173 (1979).
9. G. E. Shaw, "Inversion of optical scattering and spectral extinction measurements to recover aerosol size spectra," Appl. Opt. **18,** 988–993 (1979).
10. J. J. Michalsky, L. C. Harrison, and W. E. Berkheiser III, "Cosine response characteristics of radiometric and photometric sensors," presented at the 1992 Annual Conference of the American Solar Energy Society, Cocoa Beach, Fla., 15–18 1992.
11. L. W. Thomason, B. M. Herman, R. M. Schotland, and J. A. Reagan, "Extraterrestrial solar flux measurement limitations due to a Beer's law assumption and uncertainty in local time," Appl. Opt. **21,** 1191–1195 (1982).
12. L. Harrison and J. J. Michalsky, "Objective algorithms for the retrieval of optical depths from ground-based measurements," Appl. Opt. **33,** (1994).